J. Fluid Mech. (2008), *vol.* 595, *pp.* 409–433.
doi:10.1017/S0022112007009391 Printed in the United Kingdom

Instability of a stratified boundary layer and its coupling with internal gravity waves. Part 2. Coupling with internal gravity waves via topography

XUESONG WU[1,2] AND JING ZHANG[2]

[1]Department of Mathematics, Imperial College London London SW7 2AZ, UK
[2]Department of Mechanics, Tianjin University, China

(Received 11 April 2006 and in revised form 27 September 2007)

The aim of this paper is to show that the viscous shear instability identified in Part 1 is intrinsically coupled with internal gravity waves when a localized surface topography is present within a boundary layer. The coupling involves two aspects: receptivity and radiation. The former refers to excitation of shear instability modes by gravity waves, and the latter to emission of gravity waves by instability modes. Both physical processes are studied using triple-deck theory. In particular, the radiated gravity waves are found to produce a leading-order back action on the source, and this feedback effect, completely ignored in the acoustic analogy type of approach, is naturally taken into account by the triple-deck formalism. A by-product is that for certain incident angles, gravity waves are over-reflected by the boundary layer, i.e. the reflected waves are stronger than the incident waves.

1. Introduction

As discussed in Part 1 (Wu & Zhang 2008), a stably stratified shear flow over a topographic feature can host a variety of waves, including gravity waves, mountain lee waves, and waves arising from shear instabilities. Nonlinear solitary waves also exist in stratified flows. While these waves have their own distinct characteristics, they may be intrinsically coupled through interaction with topography. These wave activities and the interaction/coupling among them play an important role in the atmospheric boundary layer. They are thus of fundamental importance for a proper understanding, and ultimately modelling, of many boundary-layer meteorology phenomena.

Owing to the simple mechanics involved, gravity waves are particularly prevalent in the atmosphere (Gossard & Hooke 1975; Einaudi, Bedard & Finnigan 1989). These waves may be trapped within a shear layer, or freely propagating. The focus of the present work is on the latter kind, which are of special interest because they can facilitate long-range interactions. Two aspects are involved. The first is gravity-wave radiation: local flow activities may generate gravity waves, which can propagate to distant locations, both vertically and horizontally. In particular, these waves can transport horizontal momentum to high altitude, where they deposit their momentum flux when being reabsorbed by the background flow (mostly at the critical layer) or break down into small-scale turbulence. The momentum flux and resulting diffusion influence the large-scale circulation of the atmosphere (Lindzen 1981). However, gravity waves are usually filtered out in general circulation models because their time

and length scales are too small to be resolved by meteorology observation networks or by numerical modelling. Therefore an appropriate parameterization is necessary to account for the mean effect of gravity waves on the large-scale motions (Fritts 1989). For that purpose, a theoretical understanding of gravity-wave generation processes is very useful.

Several mechanisms have been identified as generating propagating gravity waves. For instance, certain shear flows may support instability modes which are free propagating, and these modes in the far field acquire the character of gravity waves (Lalas & Einaudi 1976; Mastrantonio *et al.* 1976; McIntyre & Weissman 1978; Davis & Peltier 1979; Lott, Kelder & Teitelbaum 1992). Nonlinearly modulating Kelvin–Helmoholtz (K-H) instability modes may also emit long gravity waves via the so-called 'envelope radiation' mechanism (Chimonas & Grant 1984; Fritts 1984; Scinocca & Ford 2000). Gravity waves may be generated when a steady or unsteady airflow interacts with topography (Smith 1979). Other mechanisms include geostrophic adjustment (e.g. Fritts & Luo 1992) and thermal convection. Gravity waves generated by a convectively unstable boundary layer were simulated numerically by Clark, Hauf & Kuettner (1986) and Hauf & Clark (1989). They found that the radiated gravity waves act to organize the boundary-layer flow. Small-scale turbulence may be yet another source of gravity waves. Stein (1967) extended the acoustic analogy theory of Lighthill (1952) to estimate the gravity-wave emission by a turbulent stratified atmosphere. The expression derived for the gravity-wave power output, unfortunately, turned out to be singular in the low-frequency limit. This non-physical result implies that 'the assumption that turbulence is unaffected by the buoyancy [gravity] waves that it generates must be grossly in error' (Gossard & Hooke 1975, pp. 361), that is, the radiated waves and the source of the waves are inherently coupled. In order to resolve the physically unacceptable singularity, the back effect of the gravity waves on the source (i.e. turbulence) must be considered.

The second aspect of the long-range effect is that gravity waves originating from remote sources may provoke local events. An example of particular interest is the intermittency of nocturnal boundary layers, which refers to sporadic outbursts of turbulence (Coulter & Doran 2002; Nakmura & Mahrt 2005). Its occurrence has been attributed to some form of inherent instability and the influence of external disturbances propagating from distant locations, such as internal gravity waves, solitary wave (Sun *et al.* 2004) and density current (Sun *et al.* 2002). Such perturbations may cause intermittent turbulence either by distorting the local flow condition thereby rendering the otherwise stable flow unstable, or by exciting unstable modes which the background shear flow may support.

The present study will examine the latter scenario, which is essentially what is referred to as receptivity in the context of laminar–turbulent transition (Goldstein & Hultgren 1989 and references therein). Receptivity is the first step in a long chain of processes leading to transition of aerodynamic flows (e.g. the boundary-layer flow over an airfoil), but its possible relevance in geophysical flows has not been appreciated. To fix the idea, we take the external disturbance to be a gravity wave propagating in the free stream outside the boundary layer, and the inherent instability to be the viscous instability described in Part 1. A gravity wave in general cannot directly excite instability modes, viscous or inviscid, because they have different dispersion relations except in the exceptional case of resonant over-reflection (e.g. McIntyre & Weissman 1978; Davis & Peltier 1979; Grimshaw 1981; Lott, Kelder & Teitelbaum 1992). For a gravity wave to couple with an instability wave, a *scale-conversion mechanism* is required. This crucial mechanism can be provided by surface topography with a horizontal length scale comparable with that of the instability mode. The gravity wave,

whose frequency is taken to be in the characteristic range of the viscous instability, interacts with the mean flow generated by the topography to produce a forcing, which consists of a Fourier component in resonance with an unstable eigenmode. The latter is excited as a result. This scale-conversion mechanism is essentially the same as that in acoustic receptivity (cf. Ruban 1984; Goldstein 1985). The present work intends to add viscous instability and the concept of receptivity to the existing theoretical framework for understanding intermittent turbulence in nocturnal boundary layers. In addition to a possible role in triggering nocturnal intermittency, interaction of gravity waves with topography to generate instability waves is clearly of interest and relevance to atmospheric boundary-layer dynamics in general.

As a gravity wave propagates through a shear layer, its energy may be absorbed and reflected by a critical layer (i.e. the thin layer surrounding the level at which the base velocity equals the phase speed of the wave) (Booker & Bretherton 1967; Breeding 1971; Eltayeb & Mckenzie 1975). A phenomenon which may occur under certain conditions, is over-reflection, i.e. the reflected wave is stronger than the incident wave (Jones 1968; Breeding 1971; Eltayeb & Mckenzie 1975; Acheson 1976; Lindzen & Barker 1985). The analogous problem of an oncoming gravity wave interacting with a viscous boundary-layer flow has not been studied. Such a problem arises in the present receptivity problem. It is found that gravity waves may be over-reflected by the boundary layer for certain incident angles.

The present study will also investigate the gravity waves radiated by growing viscous instability modes. Although Part 1 shows that temporal modes with $\alpha < s$ are radiating, these are heavily damped and so the gravity waves emitted are of limited interest unless a large-amplitude disturbance is present. Moreover, in the present context, only spatial instability is appropriate, and all spatially amplifying modes are trapped within the boundary layer. We shall show that when they interact with the mean-flow generated by topography whose horizontal length scale is comparable with the wavelength of the instability modes, the resulting scattered field consists of a radiating component, which represents a gravity wave in the far field. The mechanism is entirely analogous to that proposed for the acoustic radiation of T-S waves (Wu & Hogg 2006). However, unlike acoustic waves, the radiated gravity waves have a leading-order back-effect on the source.

The rest of the paper is organized as follows. In § 2, we describe and formulate the two related problems, and specify the appropriate scalings so that triple-deck theory can be applied. The resulting system is fully nonlinear. The linearized solution for the mean-flow distortion induced by a localized topographic feature is presented. The receptivity due to the scattering of an impinging gravity wave by topography is considered in § 3, and the excited instability wave is calculated, and its possible role in nocturnal intermittency is discussed. In § 4, we consider gravity-wave radiation when an instability mode interacts with the topography. In § 5, we show that in the so-called high-frequency limit, the fully nonlinear system can be reduced to an extended Benjamin–Davis–Ono (BDO) equation with variable coefficients and forcing. A brief summary and some concluding remarks are given in § 6.

2. Description and formulation of the problems

2.1. *Description of the problems: receptivity and radiation*

We consider a two-dimensional boundary layer due to a uniform flow with a speed U_0 over a localized topographic feature on an otherwise flat terrain. The local boundary-layer thickness at the centre of the topography is assumed to be δ. As in Part 1, the flow is assumed to be incompressible, and the effect of density stratification

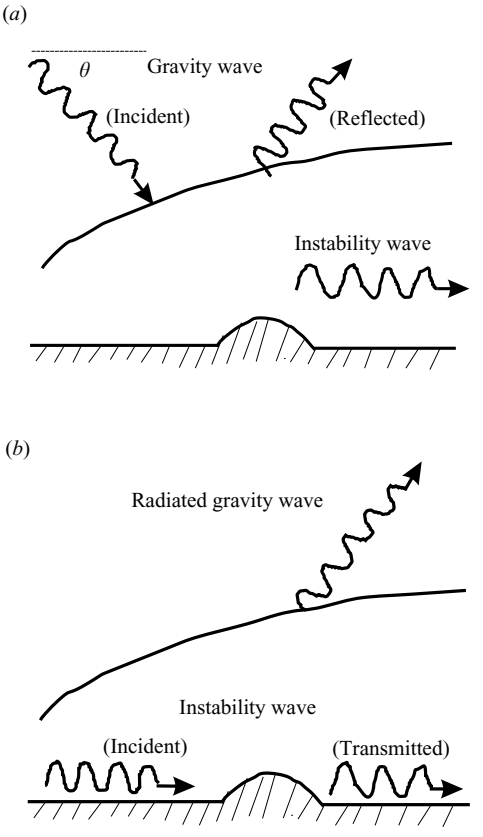

FIGURE 1. Sketch of the (*a*) receptivity and (*b*) radiation problems.

on the dynamics is accounted for by the Boussinesq approximation. The reference length and velocity are taken to be δ and U_0, respectively, and the normalized variables, (x, y) and t, and the flow quantities (u, v, p, ρ) are as introduced in (2.7) of Part 1. The Reynolds number remains as

$$R = U_0\delta/\nu,$$

and will assumed to be asymptotically large.

The height of the surface elevation h^* is assumed to be much smaller than δ, while its horizontal length scale is much larger than δ. The topography generates a local mean-flow distortion, the far field of which corresponds to mountain lee waves (Sykes 1978). The distortion attains its maximum amplitude in a thin region adjacent to the wall, and will play a crucial part in coupling the viscous instability modes and gravity waves, which otherwise would evolve independently of each other in the linear regime.

Two fundamental physical processes will be investigated. The first is concerned with the generation of the viscous instability waves, i.e. the receptivity. We assume that a gravity wave originates from a distant source. As it propagates towards the boundary layer, it will be reflected. At the same time it will generate an unsteady viscous flow within the boundary layer. This unsteady signature then interacts with the steady mean-flow distortion induced by the topography to excite instability waves (figure 1*a*).

The second process is radiation of gravity waves by the viscous instability modes, which may be viewed as an inverse problem of receptivity. Here a viscous instability wave is assumed to be present within the boundary layer upstream of the topography. As it propagates through the local non-uniform flow caused by the topography, a scattering process takes place, in which gravity waves are generated in the far field (figure 1*b*).

In order to keep the mathematical problems tractable, we shall analyse these processes assuming the base flow to be two-dimensional and laminar. Such an idealized situation may be set up in the laboratory condition, for which the theory may provide a quantitative description. However, the theoretical results should be treated as being of qualitative relevance when interpreted in the context of the atmospheric boundary layer since the flow there is in general three-dimensional, and considerable turbulence may be present.

2.2. *Formulation and scalings*

As is shown in Part 1, the viscous instability modes are a modified form of T-S waves, which can be described by triple-deck theory. Naturally, the same mathematical framework will be used to study both the receptivity and radiation problems. The notations introduced in Part 1 will be retained. The usual variables on the triple-deck scales,

$$X = R^{-1/4}x \equiv \epsilon x, \quad T = R^{-1/2}t \equiv \epsilon^2 t, \tag{2.1}$$

are introduced, where $\epsilon = R^{-1/4}$. The stratification parameter S is assumed to be a constant, and is scaled as

$$S = \epsilon s$$

so that the buoyancy term occurs in the upper deck only (Sykes 1978, 1980).

In the linear regime, gravity waves and instability modes satisfy their own dispersion relations, and evolve independently. The two are coupled in the presence of topography because the latter plays the role of a scatter: an incoming gravity (instability) wave is scattered to an instability (gravity) wave.

For topography to facilitate substantial energy transfer between gravity waves and unstable modes, its horizontal length scale is of crucial importance. In receptivity, the frequency of the gravity wave ω^* typically must scale as

$$\omega^* \sim 2\pi R^{-1/2}U_0/\delta, \tag{2.2}$$

and it follows that topography must have a horizontal length scale

$$L^* \sim R^{1/4}\delta, \tag{2.3}$$

so that the forcing resulting from their mutual interaction consists of a Fourier spectral component in resonance with a T-S wave. Similar to the acoustic radiation of T-S waves considered in Wu & Hogg (2006), for instability modes to be able to radiate gravity waves efficiently, they must undergo distortion over a length scale comparable with their wavelengths. Thus in both problems, the shape can be specified by a function of X, $y^* = h^*F(X)$ say. In order to comply with triple-deck theory, the height of the topography, h^*, is scaled as (cf. Sykes 1978)

$$h^*/\delta = \epsilon h, \tag{2.4}$$

so that the topography is described by

$$y = \epsilon h F(X),$$

where the scaled elevation $h=(h^*/\delta)R^{1/4}$ is $O(1)$ or smaller when (2.2) and (2.3) hold. In the high-frequency/short-wavelength limit corresponding to $\omega^* \gg 2\pi R^{-1/2}U_0/\delta$ and $L^* \ll R^{1/4}\delta$, h may be allowed to be much greater than order one; this case will be discussed further in § 5.

In the receptivity problem, the wavelength of the oncoming gravity wave is assumed to be comparable with those of T-S waves, although longer wavelengths are allowed. On the other hand, in the radiation problem, the gravity-wave field generated by the instability modes turns out to have $O(R^{1/4}\delta)$ length also. Therefore all the flow physics of interest occurs on the scales of $X=O(1)$ and $T=O(1)$, and are fully described by triple-deck structure.

The particular phenomenon, to which the viscous instability and the receptivity may be relevant, is intermittent turbulence in nocturnal boundary layers, which often occurs in a layer beneath the maximum of the low-level jet. In the observations reported by Sun *et al.* (2004), the width of this layer was about 100 m and the wind speed at the outer edge was about $7\,\mathrm{m\,s^{-1}}$, suggesting a Reynolds number of $O(10^7)$. Thus a surface elevation h^* of a few metres over a horizontal distance L^* up to a few kilometres would broadly fit the required scaling (2.4) and (2.3), or its suitable short-wavelength limit.

The dominant interactions of the topography with the gravity-wave signature (in the receptivity problem), and with the instability modes (in the radiation problem), take place within the lower deck, where

$$Y = y/\epsilon = O(1).$$

The solution expands as

$$(u, v, p, \rho) = \epsilon(U, \epsilon^2 V, \epsilon P, \rho) + \cdots, \tag{2.5}$$

where the amplitude of the perturbation is chosen so that the rescaled quantities (U, V, P) are governed by the fully nonlinear triple deck equations

$$\left.\begin{aligned} \frac{\partial U}{\partial T} + U\frac{\partial U}{\partial X} + V\frac{\partial U}{\partial Y} &= -\frac{\partial P}{\partial X} + \frac{\partial^2 U}{\partial Y^2}, \\ \frac{\partial U}{\partial X} + \frac{\partial V}{\partial Y} &= 0. \end{aligned}\right\} \tag{2.6}$$

These equations can be linearized subsequently for weaker disturbances. At the ground surface, U and V satisfy the no-slip and no-penetration boundary conditions,

$$U = V = 0 \quad \text{at} \quad Y = hF(X). \tag{2.7}$$

The main and upper decks are linear to leading-order with the nonlinear effect contributing small corrections of $O(\epsilon)$ and $O(\epsilon^2)$, respectively. The main deck has the solution given by (3.5) and (3.6) in Part 1. Matching ϵU with the main-deck solution requires

$$U \to \lambda(Y + A(X, T)) \quad \text{as} \quad Y \to \infty, \tag{2.8}$$

where function $A(X, T)$ is the displacement. The main deck acts to transmit the displacement to the upper deck, where $\tilde{y}=\epsilon y = O(1)$. The solution takes the same form as (3.8) in Part 1, and the governing equations are as given by (3.9)–(3.12) there but with $u_\infty = 1$. At present, it suffices to note that the rescaled pressure $\hat{P}(X, T, \tilde{y})$

satisfies the equation

$$\frac{\partial^2 \hat{P}}{\partial X^2} + \frac{\partial^2 \hat{P}}{\partial \tilde{y}^2} + s^2 \hat{P} = 0, \tag{2.9}$$

and the boundary condition

$$\frac{\partial \hat{P}}{\partial \tilde{y}} = (A_{XX} + s^2 A) \quad \text{at} \quad \tilde{y} = 0. \tag{2.10}$$

The pressure in the lower and main decks, P, is related to $\hat{P}$ via

$$P = \hat{P}(X, T, 0). \tag{2.11}$$

The coupling between the viscous flow in the lower deck and the inviscid motion flow the upper deck is facilitated by (2.10) and (2.11).

In the presence of an ambient disturbance, $\hat{P}$ must satisfy a far-field condition of the form

$$\hat{P} \to P_{\mathscr{I}}(X, T, \tilde{y}) + P_{\mathscr{R}} \quad \text{as} \quad X^2 + \tilde{y}^2 \to \infty, \tag{2.12}$$

where $P_{\mathscr{I}}$ represents an incident perturbation, and $P_{\mathscr{R}}$ stands for outgoing disturbances, which may include mountain lee waves, the reflected and/or scattered waves from the boundary layer; $P_{\mathscr{R}}$ is to be found as part of the solution. The specification of $P_{\mathscr{I}}$ depends on the nature of the external disturbance being present. For gravity waves propagating from a distant source, $P_{\mathscr{I}}$ can be represented as a superposition of Fourier components, i.e.

$$P_{\mathscr{I}} = \int_{-\infty}^{\infty} \mathscr{P}_{\infty}(\alpha, T) \mathrm{e}^{\mathrm{i}(\alpha X - \beta \tilde{y})} \mathrm{d}\alpha, \tag{2.13}$$

where $\beta = (s^2 - \alpha^2)^{1/2}$ is the dispersion relation for relatively low-frequency waves, which appear as quasi-steady in the upper deck. A gravity wave is composed of the components with $|\alpha| < s$ only, i.e. $\mathscr{P}_{\infty} = 0$ if $|\alpha| > s$, and a plus sign is chosen for β to ensure that the incident wave has a negative group velocity.

The system consisting of (2.6)–(2.13) describes the generation of instability waves as well as radiation of gravity waves; in the latter problem, $P_{\mathscr{I}}$ must be removed. In order to close the system, it is necessary to specify the upstream conditions for (U, V, A, P) as $X \to -\infty$. For the receptivity problem, the flow upstream corresponds to the signature of the gravity wave entrained into the boundary layer, whereas for the radiation problem, the upstream perturbation consists of a viscous instability mode.

We may solve the upper-deck equation (2.9) analytically to obtain a displacement–pressure relation. Let $\hat{P} = P_{\mathscr{I}} + Q$. Then Q is governed by (2.9), but satisfies the boundary condition

$$\frac{\partial Q}{\partial \tilde{y}} = (A_{XX} + s^2 A) - P_{\mathscr{I}, \tilde{y}}(X, T, 0) \quad \text{at} \quad \tilde{y} = 0, \tag{2.14}$$

and also as a far-field condition, that Q either decays or corresponds to an outgoing wave. The resulting system can be solved by using a Fourier transform to obtain

$$Q(X, T, \tilde{y}) = \int_{-\infty}^{\infty} \mathscr{P}_{\infty}(\alpha, T) \mathrm{e}^{\mathrm{i}(\alpha X + \beta \tilde{y} - \omega T)} \mathrm{d}\alpha + \int_{-\infty}^{\infty} (-\mathrm{i}m) a(k) \mathrm{e}^{\mathrm{i}(m\tilde{y} + kX)} \mathrm{d}k, \tag{2.15}$$

where $a(k)$ denotes the Fourier transform of A, and $m = (s^2 - k^2)^{1/2}$ with the branch being defined in the same way as in Part 1. Taking the limit $\tilde{y} \to 0$ in $\hat{P} = (P_{\mathscr{I}} + Q)$

and noting (2.11), we have

$$P(X,T) = 2P_{\mathscr{I}}(X,T,0) + \int_{-\infty}^{\infty} \mathscr{G}(X;\xi)(A_{\xi\xi}(\xi,T) + s^2 A(\xi,T))\,\mathrm{d}\xi, \tag{2.16}$$

where $\mathscr{G}(X;\xi)$ is given by (3.17) in Part 1. This is an inhomogeneous pressure-displacement relation, in which the forcing term, $2P_{\mathscr{I}}$, characterizes the external perturbation.

Relation (2.16) and equations (2.6)–(2.8) form a more compact formulation of the problem. The system is fully nonlinear for $h = O(1)$ and $P_{\mathscr{I}} = O(1)$, and requires a numerical attack. In the so-called high-frequency limit, the system can be simplified to an extended BDO equation with forcing. Before turning to this nonlinear case in § 5, we shall assume, in the rest of this section and throughout §§ 3 and 4, that $h \ll O(1)$ and $P_{\mathscr{I}} \ll O(1)$, for which the system can be linearized and solved analytically.

2.3. *Linear solution for the steady flow induced by topography*

Assume that $h \ll O(1)$ and $P_{\mathscr{I}} \sim \tilde{\epsilon} \ll O(1)$. Both the topography-induced steady flow, $h(\tilde{u}_m, \tilde{v}_m, \tilde{a}_m, \tilde{p}_m)$ say, and the unsteady signature of the gravity wave, $\tilde{\epsilon}(\tilde{u}_g, \tilde{v}_g, \tilde{a}_g, \tilde{p}_g)$ say, appear as small perturbations to the background flow. The total flow field can be decomposed as

$$(U, V, A, P) = (\lambda Y, 0, 0, 0) + h(\tilde{u}_m, \tilde{v}_m, \tilde{a}_m, \tilde{p}_m) + \tilde{\epsilon}(\tilde{u}_g, \tilde{v}_g, \tilde{a}_g, \tilde{p}_g) + \cdots. \tag{2.17}$$

In this section, we consider $(\tilde{u}_m, \tilde{v}_m, \tilde{a}_m, \tilde{p}_m)$. They satisfy the steady linearized version of (2.6)–(2.8), which are Fourier transformed to (Sykes 1978)

$$\left.\begin{aligned} \mathrm{i}k\lambda Y\hat{u}_m + \lambda\hat{v}_m &= -\mathrm{i}k\hat{p}_m + \hat{u}_m'', \\ \mathrm{i}k\hat{u}_m + \hat{v}_m' &= 0, \\ \hat{u}_m = -\lambda\hat{F}, \quad \hat{v}_m &= 0 \quad \text{at} \quad Y = 0, \\ \hat{u}_m &\to \lambda\hat{a}_m \quad \text{as} \quad Y \to \infty, \end{aligned}\right\} \tag{2.18}$$

where $(\hat{u}_m, \hat{v}_m, \hat{a}_m, \hat{p}_m)$ denote the flow field in spectral space. The steady part of the pressure–displacement relation (2.16) gives

$$\hat{p}_m = -\mathrm{i}m\hat{a}_m \quad \text{with} \quad m = (s^2 - k^2)^{1/2}, \tag{2.19}$$

where the branch is defined in the same manner as in Part 1 and Sykes (1978).

The solution is found as (Sykes 1978)

$$\left.\begin{aligned} \hat{p}_m(k) &= -k^{-2}(\mathrm{i}k\lambda)^{5/3}\mathrm{Ai}'(0)\lambda\hat{F}/\mathscr{D}, \\ \hat{u}_m(k,Y) &= \lambda\hat{F}\Big\{\frac{1}{\mathscr{D}}\int_0^{\eta}\mathrm{Ai}(\eta)\mathrm{d}\eta - 1\Big\}, \\ \hat{v}_m(k,Y) &= \frac{1}{\lambda}\Big\{\hat{u}_m'' - \mathrm{i}k\lambda Y\hat{u}_m - \mathrm{i}k\hat{p}_m\Big\}, \end{aligned}\right\} \tag{2.20}$$

with $\eta = (\mathrm{i}k\lambda)^{1/3}Y$, and

$$\mathscr{D}(k) = \int_0^{\infty}\mathrm{Ai}(\eta)\mathrm{d}\eta - \lambda(\mathrm{i}k\lambda)^{2/3}\mathrm{Ai}'(0)/(km). \tag{2.21}$$

3. Receptivity: excitation of instability waves

Receptivity involves a gravity wave interacting with the topography-induced local mean-flow distortion (figure 1*a*). The interaction generates a scattered field. Thus the

total flow field can be expanded as

$$(U, V, A, P) = (\lambda Y, 0, 0, 0) + h(\tilde{u}_m, \tilde{v}_m, \tilde{a}_m, \tilde{p}_m) + \tilde{\epsilon}(\tilde{u}_g, \tilde{v}_g, \tilde{a}_g, \tilde{p}_g) + \tilde{\epsilon}h(\tilde{u}_s, \tilde{v}_s, \tilde{a}_s, \tilde{p}_s) + \cdots. \tag{3.1}$$

The scattered field $(\tilde{u}_s, \tilde{v}_s, \tilde{a}_s, \tilde{p}_s)$ consists of growing instability modes, which will become dominant downstream (cf. Ruban 1984; Goldstein 1985).

3.1. *Unsteady gravity wave solution: entrainment and reflection*

As a gravity wave impinges on a boundary layer, its energy partly penetrates into the layer, and is partly reflected. In order to calculate the instability mode to be excited, it is necessary first to find the solution for the signature of the unsteady gravity wave entrained into the boundary layer. Since the gravity wave is linear, we consider a single Fourier mode by assuming that

$$P_{\mathscr{I}} = \tilde{\epsilon}\, p_\infty e^{i(\alpha X - \beta\tilde{y} - \omega T)} + \text{c.c.}$$

We ignore the transient process, and seek the 'steady-state' solution that is established a long time after the gravity has arrived. The solution can be written as

$$(\tilde{u}_g, \tilde{v}_g, \tilde{a}_g, \tilde{p}_g) = (\hat{u}_g(Y), \hat{v}_g(Y), \hat{a}_g, \hat{p}_g)e^{i(\alpha X - \omega T)} + \text{c.c.}$$

Instead of using the pressure–displacement relation (2.16), we reconsider the solution to (2.9) in the upper deck, since the physical nature of the solution can be more readily appreciated. The solution may be expressed as

$$\hat{P} = p_\infty(e^{-i\beta\tilde{y}} + \mathscr{R}e^{i\beta\tilde{y}})e^{i(\alpha X - \omega T)} + \text{c.c.}$$

where the constant $\mathscr{R}$ is recognized as the *reflection coefficient*, which is to be found as part of the solution. It follows from (2.11) and (2.10) that

$$\hat{p}_g = (1 + \mathscr{R})p_\infty, \quad (s^2 - \alpha^2)\hat{a}_g = -i\beta(1 - \mathscr{R})p_\infty.$$

Elimination of p_∞ yields

$$\hat{p}_g = \frac{i\beta(1 + \mathscr{R})}{1 - \mathscr{R}}\hat{a}_g. \tag{3.2}$$

In passing, it may be noted that had we used (2.16) instead, then

$$\hat{p}_g = 2p_\infty - i\beta\hat{a}_g = p_\infty + (p_\infty - i\beta\hat{a}_g),$$

where the second term on the right-hand side stands for the reflected wave. Then on identifying the reflection coefficient $\mathscr{R} = (p_\infty - i\beta\hat{a}_g)/p_\infty$, the same relation (3.2) would have been derived.

The unsteady viscous flow in the lower deck remains to be considered. It which is governed by the linearized boundary-layer equations

$$-i\omega\hat{u}_g + i\alpha\lambda Y\hat{u}_g + \lambda\hat{v}_g = -i\alpha\hat{p}_g + \hat{u}_g'', \tag{3.3}$$

$$i\alpha\hat{u}_g + \hat{v}_g' = 0, \tag{3.4}$$

subject to the matching condition

$$\hat{u}_g \to \lambda\hat{a}_g \quad \text{as} \quad Y \to \infty, \tag{3.5}$$

and the boundary condition

$$\hat{u}_g = 0, \quad \hat{v}_g = 0 \quad \text{at} \quad Y = 0. \tag{3.6}$$

Differentiating (3.3) with respect to Y and using (3.4) to eliminate $\widehat{v}_g$ yields

$$\widehat{u}_g''' + \mathrm{i}(\omega - \alpha\lambda Y)\widehat{u}_g' = 0. \tag{3.7}$$

The solution to this equation with boundary condition (3.6) is

$$\widehat{u}_g = C\int_{\zeta_0}^{\zeta} \mathrm{Ai}(\zeta)\mathrm{d}\zeta, \tag{3.8}$$

where C is an arbitrary constant, and

$$\zeta = (\mathrm{i}\alpha\lambda)^{1/3}Y + \zeta_0, \qquad \zeta_0 = -\mathrm{i}\omega(\mathrm{i}\alpha\lambda)^{-2/3}. \tag{3.9}$$

Note that setting $Y = 0$ in (3.3) yields $\widehat{u}_g''(0) = \mathrm{i}\alpha\widehat{p}_g$. Use of this and (3.5) gives

$$C(\mathrm{i}\alpha\lambda)^{2/3}\mathrm{Ai}'(\zeta_0) = \mathrm{i}\alpha\widehat{p}_g, \quad C\int_{\zeta_0}^{\infty} \mathrm{Ai}(\zeta)\mathrm{d}\zeta = \lambda\widehat{a}_g. \tag{3.10}$$

From (3.2) and (3.10), we find that the reflection coefficient

$$\mathscr{R} = 1 - 2\int_{\zeta_0}^{\infty} \mathrm{Ai}(\zeta)\mathrm{d}\zeta/\Delta_g(\alpha, \omega), \tag{3.11}$$

and $C = 2\lambda p_\infty/(\mathrm{i}\beta\Delta_g)$ so that

$$\widehat{u}_g = \frac{2\lambda p_\infty}{\mathrm{i}\beta\Delta_g}\int_{\zeta_0}^{\zeta} \mathrm{Ai}(\zeta)\mathrm{d}\zeta, \tag{3.12}$$

where we have put

$$\Delta_g(\alpha, \omega) = \int_{\zeta_0}^{\infty} \mathrm{Ai}(\zeta)\mathrm{d}\zeta - \lambda(\mathrm{i}\alpha\lambda)^{2/3}\mathrm{Ai}'(\zeta_0)/(\alpha\beta). \tag{3.13}$$

The reflection coefficient of the gravity wave, $\mathscr{R}$, is of considerable interest. As it stands, it depends on three parameters: ω, s and α. Alternatively, it is more illuminating to introduce the incident angle θ, i.e. the angle that the wave vector makes with the horizontal (see figure 1*a*). It is defined as

$$\tan\theta = \frac{\beta}{\alpha} = \frac{\sqrt{s^2 - \alpha^2}}{\alpha}, \tag{3.14}$$

and we treat $\mathscr{R} = \mathscr{R}(\omega, s, \theta)$ as a function of ω, s and θ.

It is worth noting that in the general case of an impinging wavepacket, the reflection of each of its constitutnent Fourier components would still be described by the reflection coefficient given here. The reflected wavepacket can be computed by taking Fourier inversion (along a contour that respects casuality). Since reflection of a wavepacket is a transient process, it must be characterized by a time scale. Extracting this and other specific features requires further investigation, and will not pursued in the present paper.

3.2. *The scattered wave field*

We now consider the scattered field $(\tilde{u}_s, \tilde{v}_s, \tilde{a}_s, \tilde{p}_s)$ in (3.1). Since the problem is linear, the solution will have a harmonic time dependence, i.e.

$$(\tilde{u}_s, \tilde{v}_s, \tilde{a}_s, \tilde{p}_s) = (u_s, v_s, a_s, p_s)\mathrm{e}^{-\mathrm{i}\omega T} + \mathrm{c.c.}$$

Then (u_s, v_s, a_s, p_s) satisfies the inhomogeneous linearized boundary-layer equations

$$-\mathrm{i}\omega u_s + \lambda Y\frac{\partial u_s}{\partial X} + \lambda v_s = -\frac{\partial p_s}{\partial X} + \frac{\partial^2 u_s}{\partial Y^2} - N\mathrm{e}^{\mathrm{i}\alpha X}, \quad \frac{\partial u_s}{\partial X} + \frac{\partial v_s}{\partial Y} = 0, \tag{3.15}$$

where we have put

$$N(X,Y)=\left\{\mathrm{i}\alpha u_m\widehat{u}_g+v_m\widehat{u}_g'+\widehat{u}_g\frac{\partial u_m}{\partial X}+\widehat{v}_g\frac{\partial u_m}{\partial Y}\right\}. \tag{3.16}$$

The pressure–displacement relation (2.16) becomes

$$p_s=\int_{-\infty}^{\infty}\mathscr{G}(X;\xi)\big(a_s''(\xi)+s^2a_s(\xi)\big)\,\mathrm{d}\xi. \tag{3.17}$$

The boundary and matching conditions are approximated as

$$u_s(X,0)=-\widehat{u}_g'(0)\mathrm{e}^{\mathrm{i}\alpha X}F(X),\qquad v_s=0\quad\text{at}\quad Y=0, \tag{3.18}$$

$$u_s\to\lambda a_s\quad\text{as}\quad Y\to\infty. \tag{3.19}$$

The linearized triple-deck system (3.15)–(3.19) is similar to that which arises in the acoustic receptivity problem (Goldstein 1985), and can be solved by Fourier transform. Let $(\widehat{u}_s,\widehat{v}_s,\widehat{a}_s,\widehat{p}_s)$ denote the flow quantities in the Fourier spectral space. Then system (3.15)–(3.19) is transformed to

$$-\mathrm{i}\omega\widehat{u}_s+\mathrm{i}k\lambda Y\widehat{u}_s+\lambda\widehat{v}_s=-\mathrm{i}k\widehat{p}_s+\frac{\partial^2\widehat{u}_s}{\partial Y^2}-\widehat{N}, \tag{3.20}$$

$$\mathrm{i}k\widehat{u}_s+\frac{\partial\widehat{v}_s}{\partial Y}=0, \tag{3.21}$$

$$\widehat{p}_s=-\mathrm{i}m\widehat{a}_s, \tag{3.22}$$

$$\widehat{u}_s(0)=-\widehat{u}_g'(0)\widehat{F}(k-\alpha),\quad \widehat{v}_s(0)=0, \tag{3.23}$$

$$\widehat{u}_s\to\lambda\widehat{a}_s\quad\text{as}\quad Y\to\infty, \tag{3.24}$$

where

$$\widehat{N}(k,Y)=\mathrm{i}\alpha\widehat{u}_m\widehat{u}_g+\mathrm{i}(k-\alpha)\widehat{u}_g\widehat{u}_m+\widehat{v}_m\widehat{u}_g'+\widehat{v}_g\widehat{u}_m'.$$

The quantities with subscript m are evaluated at $(k-\alpha)$.

Again differentiating (3.20) with respect to Y and using (3.21) to eliminate $\widehat{v}_s$, we obtain

$$\widehat{u}_s'''+\mathrm{i}(\omega-k\lambda Y)\widehat{u}_s'=\widehat{N}_Y, \tag{3.25}$$

where

$$\widehat{N}_Y=\mathrm{i}\alpha\widehat{u}_m\widehat{u}_s'(Y)+\mathrm{i}(k-\alpha)\widehat{u}_s(Y)\widehat{u}_m'+\widehat{v}_m\widehat{u}_s''(Y)+\widehat{v}_s(Y)\widehat{u}_m''. \tag{3.26}$$

Now setting $Y=0$ in (3.20) and using (3.23) gives

$$\widehat{u}_s''(0)=\mathrm{i}k\widehat{p}_s+\mathrm{i}\omega\widehat{u}_g'(0)\widehat{F}(k-\alpha). \tag{3.27}$$

This boundary condition replaces $\widehat{v}_s(0)=0$.

Now putting (cf. Goldstein 1985)

$$\widehat{u}_s=\widehat{u}_1+\frac{1}{\lambda}\int_0^Y\big(\widehat{u}_g''\widehat{u}_m+\widehat{u}_g\widehat{u}_m''\big)\,\mathrm{d}Y, \tag{3.28}$$

and substituting it into (3.25), we find that $\widehat{u}_1$ satisfies

$$\widehat{u}_1'''+\mathrm{i}(\omega-k\lambda Y)\widehat{u}_1'=\widehat{G}(Y), \tag{3.29}$$

where

$$\widehat{G}(Y)=-\lambda^{-1}\big(2\widehat{u}_g'''\widehat{u}_m'+2\widehat{u}_g'\widehat{u}_m'''+\widehat{u}_g''\widehat{u}_m''(0)+\widehat{u}_g''(0)\widehat{u}_m''\big). \tag{3.30}$$

By using the two homogeneous solutions to the Airy equation, $\mathrm{Ai}(\xi)$ and $\mathrm{Bi}(\xi)$, the solution to the inhomogeneous equation (3.29) that remains bounded as $Y \to \infty$ can be expressed as

$$\widehat{u}_1' = -(\mathrm{i}k\lambda)^{-1/3}\pi\left\{\mathrm{Ai}(\xi)\int_0^Y \mathrm{Bi}(\tilde{\xi})\widehat{G}(\tilde{Y})\,\mathrm{d}\tilde{Y} - \mathrm{Bi}(\xi)\int_\infty^Y \mathrm{Ai}(\tilde{\xi})\widehat{G}(\tilde{Y})\,\mathrm{d}\tilde{Y}\right\} + C_1(\mathrm{i}k\lambda)^{1/3}\mathrm{Ai}(\xi), \tag{3.31}$$

where C_1 a function of k to be found, and

$$\xi = (\mathrm{i}k\lambda)^{1/3}Y + \xi_0, \qquad \xi_0 = -\mathrm{i}\omega(\mathrm{i}k\lambda)^{-2/3}. \tag{3.32}$$

We integrate (3.31) once using boundary condition (3.23) to obtain $\widehat{u}_1$, which is then inserted into (3.28) to give

$$\begin{aligned}\widehat{u}_s = {} & -(\mathrm{i}k\lambda)^{-1/3}\pi\int_0^Y\left\{\mathrm{Ai}(\xi)\int_0^Y \mathrm{Bi}(\tilde{\xi})\widehat{G}(\tilde{Y})\,\mathrm{d}\tilde{Y} - \mathrm{Bi}(\xi)\int_\infty^Y \mathrm{Ai}(\tilde{\xi})\widehat{G}(\tilde{Y})\,\mathrm{d}\tilde{Y}\right\}\mathrm{d}Y \\ & + C_1\int_{\xi_0}^{\xi}\mathrm{Ai}(\xi)\mathrm{d}\xi + \frac{1}{\lambda}\int_0^Y\left(\widehat{u}_g''\widehat{u}_m + \widehat{u}_g\widehat{u}_m''\right)\mathrm{d}Y - \widehat{u}_g'(0)\widehat{F}(k-\alpha).\end{aligned} \tag{3.33}$$

Solution (3.33) is then used in (3.27) and (3.24). The resulting equations and (3.22) are solved to obtain

$$\begin{aligned}\widehat{a}_s = \frac{\mathrm{Ai}'(\xi_0)}{km\Delta(k,\omega)}\Bigg\{ & \int_0^\infty K(\xi,\xi_0)\widehat{G}(Y)\mathrm{d}Y + \frac{2}{\lambda}(\mathrm{i}k\lambda)^{2/3}\int_0^\infty \widehat{u}_g'\widehat{u}_m'\mathrm{d}Y \\ & + \frac{1}{\lambda}\left(\widehat{u}_g''(0)\widehat{u}_m'(0) + \widehat{u}_g'(0)\widehat{u}_m''(0)\right)\tilde{\mathscr{R}}\Bigg\},\end{aligned} \tag{3.34}$$

where

$$\Delta(k,\omega) = \int_{\xi_0}^\infty \mathrm{Ai}(\xi)\mathrm{d}\xi - \lambda(\mathrm{i}k\lambda)^{2/3}\mathrm{Ai}'(\xi_0)/(km), \tag{3.35}$$

is the dispersion relation of the viscous instability (see Part 1). Here we have introduced

$$K(\xi,\xi_0) \equiv \pi\frac{\mathrm{Ai}'(\xi_0)\mathrm{Gi}(\xi) - \mathrm{Gi}'(\xi_0)\mathrm{Ai}(\xi)}{\mathrm{Ai}'(\xi_0)}, \quad \tilde{\mathscr{R}} = \int_{\xi_0}^\infty \mathrm{Ai}(\xi)\mathrm{d}\xi/\mathrm{Ai}'(\xi_0), \tag{3.36}$$

with Gi and Gi′ denoting the combinations of Airy functions and Airy-function integrals defined by Abramowitz & Stegun (1964, p. 449).

3.3. *The coupling coefficient*

The solution in physical space can be obtained by inverting the Fourier transforms. For the displacement, we have

$$\tilde{a}_s(X,T) = \frac{1}{(2\pi)^{1/2}}\int_{-\infty}^\infty \mathrm{e}^{\mathrm{i}(kX-\omega T)}\widehat{a}_s(k)\,\mathrm{d}k. \tag{3.37}$$

The integrand has poles at the values of k which are roots of the dispersion relation (3.35), i.e.

$$\Delta(k,\omega) = 0. \tag{3.38}$$

The instability waves correspond to the contribution to the integral from these poles (Ruban 1984; Goldstein 1985; Wu 2001), which can be calculated by using the residual theorem. Of interest is the most unstable (or least stable) mode, which corresponds

to the pole with the smallest imaginary part. Let a_{TS} denote this contribution. Then from (3.34) it can be derived that

$$a_{TS}(X,T) = \frac{1}{(2\pi)^{1/2}}\widehat{F}(k-\alpha)\Lambda(\omega,\alpha)\mathrm{e}^{\mathrm{i}(kX-\omega T)}, \tag{3.39}$$

where we have put

$$\Lambda(\omega,\alpha) = \frac{\mathrm{Ai}'(\xi_0)}{km\Delta'(k,\omega)\widehat{F}(k-\alpha)}\left\{\int_0^\infty K(\xi,\xi_0)\widehat{G}(Y)\,\mathrm{d}Y + \frac{2}{\lambda}(\mathrm{i}k\lambda)^{2/3}\int_0^\infty \widehat{u}_g'\widehat{u}_m'\,\mathrm{d}Y \right.$$
$$\left. + \frac{1}{\lambda}\left(\widehat{u}_g''(0)\widehat{u}_m'(0) + \widehat{u}_g'(0)\widehat{u}_m''(0)\right)\tilde{\mathscr{R}}\right\}, \tag{3.40}$$

where Δ' stands for the derivative of Δ with respect to k. The factor Λ is a function of the horizontal wavenumber α and frequency ω of the incoming gravity wave, but independent of the geometry of the topography. It measures the efficiency of gravity waves in exciting instability modes, and is usually referred to as the *coupling coefficient*.

The result (3.39) indicates the absolute amplitude of the instability mode excited is proportional to $\widehat{F}(k-\alpha)$. The role of the horizontal scale of surface topography transpires when one considers $\widehat{F}(k-\alpha)$ for a Gaussian shape,

$$F(X) = \exp(-X^2/d^2), \tag{3.41}$$

where d is the (scaled) horizontal scale. It follows that $\widehat{F}(k-\alpha) \sim d\exp\{-d^2(k-\alpha)^2\}$. Clearly, $\widehat{F}(k-\alpha)$ attains its maximum when $d \sim (k-\alpha)^{-1}$, i.e. when $d \sim k^{-1}$, since α is $O(k)$ or smaller. The result indicates that the horizontal length scale of topography must be comparable with the characteristic wavelength of the instability modes, a conclusion that holds for isolated topography of an arbitrary shape. If topographic variation is over a much longer length scale (i.e. $d \gg k^{-1}$), the amplitude of the excited instability mode could be extremely small, indeed exponentially small for Gaussian and many other shapes.

3.4. *Numerical results*

Numerical calculations were performed to compute the reflection coefficient $\mathscr{R}$ given by (3.11) and the coupling coefficient Λ given by (3.40). The Airy functions, function Gi, and their derivatives were evaluated numerically by integrating the equations that they satisfy using a fourth-order Runge–Kutta method. The integrations (in the complex plane) were started using the large or small variable asymptotic approximations as initial conditions.

Figure 2(*a*) shows how $|\mathscr{R}|$ varies with the horizontal wavenumber α of the incoming wave for fixed frequencies. For the majority of α, $|\mathscr{R}| < 1$, indicating that the boundary layer absorbs some of the incident gravity wave energy. However, for each frequency there exist a range of α values, for which $|\mathscr{R}| > 1$, implying that the wave reflected by the viscous boundary layer is stronger than the incident wave. This is the so-called 'over-reflection' phenomenon. The figure shows that for the majority of α, higher-frequency gravity waves have larger $|\mathscr{R}|$, but over-reflection is stronger for lower frequencies. As mentioned in § 1, there have been many studies of gravity-wave reflection by critical layers, where over-reflection may occur. Interaction of gravity waves with viscous boundary layers is obviously an important process, but does not appear to have received much attention. We are not aware of any report of over-reflection in this context.

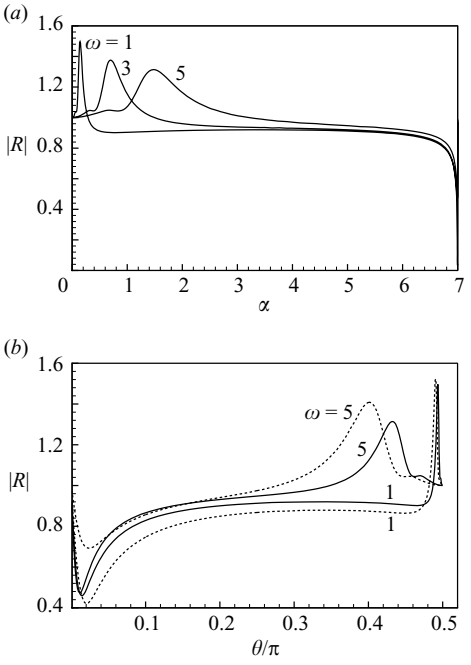

FIGURE 2. The reflection coefficient $|\mathscr{R}|$. (*a*) $|\mathscr{R}|$ *vs.* α for $\omega = 1, 3, 5$, and the stratification parameter $s = 7$. (*b*) $|\mathscr{R}|$ *vs.* θ (the incident angle) for $\omega = 1, 5$ and – – –, $s = 5$; ——, 7.

It may be tempting to interpret the observed over-reflection in terms of a resonance between a particular gravity wave and a neutrally stable mode (cf. McIntyre & Weissman 1978; Davis & Peltier 1979). However, no such a resonance is possible in our problem because the marginally stable mode is trapped within the boundary layer whilst all radiating modes are damped. Indeed, had such a resonance occurred, $|\mathscr{R}|$ would have exhibited an infinite as opposed to a finite peak.

Since the α values for which over-reflection occurs is rather small, the corresponding incident angles θ must be quite close to $\pi/2$ (see (3.14)). This is illustrated in figure 2(*b*), where $|\mathscr{R}|$ is re-plotted against θ for fixed $\omega = 1$ and 5. Indeed $|\mathscr{R}|$ attains its maximum at an angle in the vicinity of $\pi/2$. Nevertheless, there is a small yet finite difference, indicating that the maximum is not an artefact of $\pi/2$ being a singular limit. The sharp peak for low-frequency waves indicates that over-reflection is sensitive to the incident angle. The effect of stratification on reflection is delicate, depending on the frequency and the incident angle of the gravity wave. Over the majority of incident angles, stratification tends to suppress reflection of high-frequency waves (e.g. $\omega = 5$), but enhances reflection of low-frequency waves (e.g. $\omega = 1$). This trend, however, reverses for incident angles close to $\pi/2$.

For definitiveness, the coupling coefficient $|\Lambda|$ was computed with $p_\infty = 1$. Figures 3(*a*) and (*b*) show how $|\Lambda|$ varies with α for a selection of ω. The behaviour of the the coupling coefficient is different for the decaying and growing modes. For the low-frequency decaying modes ($\omega < 5$), $|\Lambda|$ exhibits two peaks (figure 3*a*), with the sharper and dominant one occurring at α close to (but slightly less than) s, indicating that the excited T-S wave has a highly tuned response to the wavenumber α (or equivalently to the incident angle) of the gravity wave. The main peak corresponds to a gravity wave propagating almost horizontally, i.e. with $\theta \approx 0$ (see (3.14)). For the

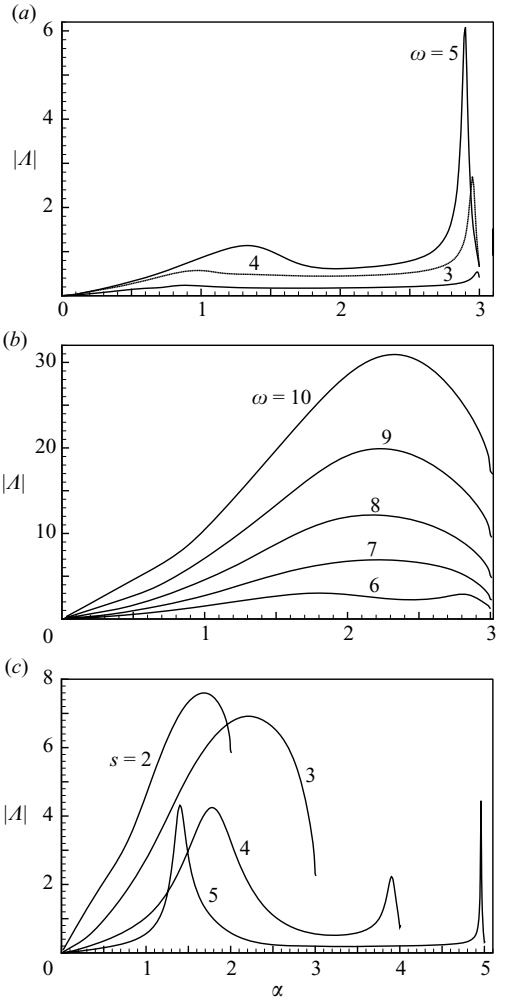

FIGURE 3. Variation of the coupling coefficient $|\Lambda|$ with α: (*a*) $s = 3$, $\omega = 3, 4, 5$ (low-frequency decaying modes); (*b*) $s = 3$, $\omega = 6, 7, 8, 9, 10$ (high-frequency growing modes); (*c*) $\omega = 7$, $s = 2, 3, 4, 5$.

unstable modes with high frequencies ($\omega > 6$), the two peaks merge (figure 3*b*). The resulting single maximum occurs at $\alpha \approx 2.3$, which corresponds to an incident angle of about 45°. Broadly speaking, high-frequency gravity waves are more efficient in exciting T-S waves.

For the major unstable frequency band, which for $s = 3$ is between $\omega = 6$ and $\omega = 12$, the coupling coefficient $|\Lambda|$ is in the range of 5–30. The ratio of the vertical velocity of a T-S wave to that of the oncoming gravity wave is $h\Lambda$, or $(h^*/\delta)R^{1/4}\Lambda$. Since the Reynolds number for atmospheric flows is usually large, the result implies that generation of instability waves is sensitive to surface topography. For $R = 10^7$, which is representative of a low-level jet, the ratio is of order one when $h^* \sim 0.01\delta$. Typically, airflows of this type occur within a layer of a few hundreds metres, and so a surface elevation of a few metres is sufficient to trigger instability modes with sizeable amplitudes.

The feature revealed by figures 3(*a*) and 3(*b*) persists for other values of s. In figure 3(*c*), the variation of $|\Lambda|$ with α is plotted for a selection of s values with a fixed $\omega = 7$. For $s = 2$ and 3, the gravity wave with $\omega = 7$ excites an unstable mode, and $|\Lambda|$ processes one peak. However, when $s = 4$, and 5, the mode excited for each α turns out to be stable, and two distinct maxima appear. For the high-frequency unstable modes, stratification tends to reduce the efficiency of the coupling for all α. However, the effect of stratification is complicated on the low-frequency stable modes. Given that these modes would experience exponential decay and that the coupling is fairly weak for them, their excitation is probably of less importance.

Taking together the results concerning the reflection and receptivity, we come to a general understanding that low-frequency gravity waves propagating almost vertically towards the boundary layer are over-reflected, whilst high-frequency components penetrate into the layer to generate instability modes.

3.5. *Receptivity and intermittent turbulence in nocturnal boundary layers*

The field investigations documented in Sun *et al.* (2004) indicate clearly that intermittent turbulence was triggered by non-local disturbances, such as solitary waves and internal gravity waves. These disturbances originate from distant locations, and propagate in the airflow at relatively high levels (about 1 km). As they descend toward the ground, they may generate conditions which support thermal or dynamic shear instabilities. Therefore, characterizing these disturbances as well as their interactions with the boundary layer and local topography is a necessary step towards understanding the onset of turbulence. Receptivity is an important aspect in these interactions.

Sun *et al.* (2004) described how a gravity wave, with a period about 10 min, propagated downward from a height of 1.5 km and triggered a major turbulence episode during CASES-99 (1999 Cooperative Atmosphere-Surface Exchange Study). High-resolution Doppler lidar revealed a well-defined wave of the same period within the boundary layer. However, it is unclear whether this wave is simply the signature of the oncoming gravity wave entrained into the boundary layer (which would mathematically correspond to the inhomogeneous solution $(\tilde{u}_g, \tilde{v}_g, \tilde{p}_g)$ described in § 3.1), or is a viscous instability mode excited by the oncoming gravity wave via a local receptivity such as that described in §§ 3.2 and 3.3. In our view, the latter is plausible. First, the long wavelength (1.2 km) and relatively small propagation speed (2 m s^{-1}, which is about 0.3 times the wind speed) are consistent with the characteristics of T-S waves. Secondly, the surface in the observation site exhibits an elevation of 6 m over a horizontal disturbance of a few hundreds meters (Nakamura & Mahrt 2005). A gravity wave may interact with such a topographical feature to generate a T-S mode. Thirdly, the low-frequency long-wavelength wave apparently modulates the onset of intermittent turbulence. The occurrence of the latter was found to be most frequent in a thin layer (about 25 m) adjacent to the ground. This is consistent with the wall-mode character of T-S waves.

Based on these observations, it may be speculated that receptivity could play a role in triggering intermittent turbulence in nocturnal boundary layers. Viscous modes excited by the present receptivity are of course not turbulence, but they may break down into small-scale motions through secondary instability, once they have grown to exceed a threshold amplitude. The requirement for a threshold implies that breakdown is likely to be sporadic, depending on the intensity of the oncoming perturbations (gravity waves) in the atmosphere as well as the local topographical conditions.

4. Radiation of gravity waves by instability modes

We now consider the situation where a viscous instability mode is already present in the boundary layer upstream of the topography (see figure 1*b*). The oncoming instability wave is scattered by the topography-induced local mean-flow distortion to radiate gravity waves to the far field. Similar to the receptivity problem considered earlier, the total flow field can be expanded as

$$(U, V, A, P) = (\lambda Y, 0, 0, 0) + h(\tilde{u}_m, \tilde{v}_m, \tilde{a}_m, \tilde{p}_m) + \tilde{\epsilon}(\widehat{u}, \widehat{v}, \widehat{a}, \widehat{p})\exp(\mathrm{i}(\alpha_{TS}X - \omega_{TS}t)) + \tilde{\epsilon}h(\tilde{u}_s, \tilde{v}_s, \tilde{a}_s, \tilde{p}_s) + \cdots, \tag{4.1}$$

where the mean-flow distortion $(\tilde{u}_m, \tilde{v}_m, \tilde{a}_m, \tilde{p}_m)$ is given in § 3 in spectral space. The only difference from receptivity is that the T-S wave signature $(\widehat{u}, \widehat{v}, \widehat{a}, \widehat{p})\exp(\mathrm{i}(\alpha_{TS}X - \omega_{TS}t))$ replaces that of the gravity wave. In the following, the subscript 'TS' will be dropped for brevity.

The solution for the instability wave is described in Part 1. In particular,

$$\widehat{u} = \int_{\eta_0}^{\eta} \mathrm{Ai}(\eta)\mathrm{d}\eta, \quad \widehat{p} = \lambda(\mathrm{i}\alpha\lambda)^{-1/3}\mathrm{Ai}'(\eta_0), \tag{4.2}$$

where

$$\eta = (\mathrm{i}\alpha\lambda)^{1/2}Y + \eta_0, \quad \eta_0 = -\mathrm{i}\omega(\mathrm{i}\alpha\lambda)^{-2/3}.$$

The frequency ω and wavenumber α satisfy the dispersion relation

$$\Delta(\alpha, \omega) \equiv \int_{\eta_0}^{\infty} \mathrm{Ai}(\eta)\mathrm{d}\eta - \frac{\lambda(\mathrm{i}\alpha\lambda)^{2/3}\mathrm{Ai}'(\eta_0)}{\alpha(s^2 - \alpha^2)^{1/2}} = 0, \tag{4.3}$$

where the branch of the square root is chosen such that T-S wave eigenfunctions in the upper deck decay exponentially (see Part 1).

4.1. *Scattering and radiation*

The main focus in the following is the scattered field, which can be written as

$$(\tilde{u}_s, \tilde{v}_s, \tilde{a}_s, \tilde{p}_s) = (u_s, v_s, a_s, p_s)\mathrm{e}^{-\mathrm{i}\omega T} + \mathrm{c.c.}$$

Then (u_s, v_s, a_s, p_s) satisfy an inhomogeneous triple-deck system similar to (3.15)–(3.19), which can be Fourier transformed to obtain the flow quantities in spectral space, which are denoted by $(\widehat{u}_s, \widehat{v}_s, \widehat{a}_s, \widehat{p}_s)$. By a similar procedure as in § 3, it can be shown that $\widehat{u}_s$ is governed by

$$\widehat{u}_s''' - \mathrm{i}(k\lambda Y - \omega)\widehat{u}_s' = (\mathrm{i}k\lambda)H, \tag{4.4}$$

supplemented by the pressure–displacement relation

$$\widehat{p}_s = -\mathrm{i}m\widehat{a}_s \quad \text{with} \quad m = (s^2 - k^2)^{1/2}. \tag{4.5}$$

Equation (4.4) is subjected to the boundary condition

$$\widehat{u}_s = -\widehat{u}'(0)\widehat{F}(k - \alpha), \quad \widehat{u}_s''(0) = \mathrm{i}\omega\widehat{u}'(0)\widehat{F}(k - \alpha) + \mathrm{i}k\widehat{p}_s, \tag{4.6}$$

and the matching condition

$$\widehat{u}_s \to \lambda\widehat{a}_s \quad \text{as} \quad Y \to \infty. \tag{4.7}$$

In (4.4), the forcing term

$$H = \frac{1}{\lambda}(\mathrm{i}k\lambda)^{-1}\{\mathrm{i}(k - \alpha)\lambda\widehat{u}\,\widehat{u}_m' + \mathrm{i}\alpha\lambda\widehat{u}'\widehat{u}_m + \widehat{u}_m''[\widehat{u}'' - \mathrm{i}(\alpha\lambda Y - \omega)\widehat{u} - \mathrm{i}\alpha\widehat{p}\,] + \widehat{u}''[\widehat{u}_m'' - \mathrm{i}(k - \alpha)\lambda Y\widehat{u}_m - \mathrm{i}(k - \alpha)\widehat{p}_m]\}, \tag{4.8}$$

where the mean-flow quantities (i.e. those with the subscript m) are evaluated at $(k-\alpha)$. Note that H decays exponentially as $Y \to \infty$. The solution to (4.4) can be expressed as (cf. Wu & Hogg 2006)

$$\widehat{u}_s = -\widehat{u}'(0)\widehat{F}(k-\alpha) + \int_{\xi_0}^{\zeta} \tilde{M}(\xi,\xi_0)\mathrm{d}\xi + \widehat{C}(k)\int_{\xi_0}^{\xi} \mathrm{Ai}(\xi)\mathrm{d}\xi, \tag{4.9}$$

where

$$\tilde{M}(\xi,\xi_0) = \pi\left\{\mathrm{Bi}(\xi)\int_{\infty}^{\xi} \mathrm{Ai}(\tilde{\xi})H(\tilde{Y})\mathrm{d}\tilde{\xi} - \mathrm{Ai}(\xi)\int_{\xi_0}^{\xi} \mathrm{Bi}(\tilde{\xi})H(\tilde{Y})\mathrm{d}\tilde{\xi}\right\} \tag{4.10}$$

with

$$\xi = (\mathrm{i}k\lambda)^{1/3}Y + \xi_0, \quad \xi_0 = -\mathrm{i}\omega(\mathrm{i}k\lambda)^{-2/3}. \tag{4.11}$$

Application of the boundary and matching conditions, (4.6) and (4.7), gives

$$\left.\begin{aligned} (\mathrm{i}k\lambda)^{2/3}\left\{\pi\mathrm{Bi}'(\xi_0)\int_{\infty}^{\xi_0}\mathrm{Ai}(\xi)H(Y)\mathrm{d}\xi + \widehat{C}(k)\mathrm{Ai}'(\xi_0)\right\} &= \mathrm{i}\omega\widehat{u}'(0)\widehat{F} + \mathrm{i}k\widehat{p}_s, \\ -\widehat{u}'(0)\widehat{F} + \int_{\xi_0}^{\infty}\tilde{M}(\xi,\xi_0)\mathrm{d}\xi + \widehat{C}(k)\int_{\xi_0}^{\infty}\mathrm{Ai}(\xi)\mathrm{d}\xi &= \lambda\widehat{a}_s. \end{aligned}\right\} \tag{4.12}$$

Eliminating $\widehat{a}_s$ and $\widehat{C}(k)$ from (4.5) and (4.12), we obtain

$$\widehat{p}_s(k) = -\frac{\mathrm{i}(\mathrm{i}k\lambda)^{2/3}\mathrm{Ai}'(\xi_0)}{k\Delta(k,\omega)}\left\{\widehat{u}'(0)\widehat{F}(1+\xi_0\tilde{\mathscr{R}}(\xi_0)) + \int_{\xi_0}^{\infty}K(\xi,\xi_0)H(Y)\mathrm{d}\xi\right\}, \tag{4.13}$$

where Δ, $K(\xi,\xi_0)$ and $\tilde{\mathscr{R}}$ are as defined by (3.35) and (3.36), respectively.

4.2. *The far field of the radiated gravity wave*

The solution in physical space for the pressure of the scattered field is given by the Fourier inversion

$$\tilde{p}_s = \frac{1}{\sqrt{2\pi}}\int_{-\infty}^{\infty}\widehat{p}_s(k)\exp(\mathrm{i}(kX + (s^2-k^2)^{1/2}\tilde{y} - \omega T))\mathrm{d}k. \tag{4.14}$$

Of particular interest is the far-field of $\tilde{p}_s$, since it corresponds to the gravity wave radiated by the viscous instability mode through scattering. Unlike scattering of a T-S wave in the unstratified case considered in Wu & Hogg (2006), the integrand in (4.14) has a stationary phase at

$$k = k_s \equiv s\cos\phi,$$

where $\phi \equiv \tan^{-1}(\tilde{y}/X)$ is the observation angle. The method of stationary phase yields

$$\tilde{p}_s = \frac{1}{\sqrt{r}}G_s(\phi;\omega,s)\exp(\mathrm{i}(sr - \omega T - \pi/4)) \quad \text{for} \quad r \equiv (X^2+\tilde{y}^2)^{1/2} \gg 1, \tag{4.15}$$

where

$$G_s(\phi;\omega,s) = -\frac{\mathrm{i}\sqrt{s}(\mathrm{i}k_s\lambda)^{2/3}\mathrm{Ai}'(\xi_0)\sin\phi}{k_s\Delta(k_s,\omega)}\left\{(1+\xi_0\tilde{\mathscr{R}}(\xi_0))\widehat{u}'(0)\widehat{F} + \int_{\xi_0}^{\infty}K(\xi,\xi_0)H(Y)\mathrm{d}\xi\right\}, \tag{4.16}$$

which characterizes the directivity and intensity of the radiated gravity-wave field. The source of the gravity wave consists of two parts: a surface source and a volumetric

source, represented, respectively, by the first and the second (integral) terms in the braces. The exponential decay of H ensures the convergence of the integral. It is worth pointing out that because of the existence of a stationary phase, only the leading-order approximation of the near-field source is required for calculating the radiated gravity wave; this is in contrast to the acoustic radiation problem considered by Wu & Hogg (2006), where the source has to be obtained up to $O(\epsilon^3)$ accuracy.

An important point is that the present triple-deck formalism has naturally included the back-effect of the radiated gravity wave on the source. This is because in the present interactive system, the viscous motion induces a displacement, which is transmitted to the upper deck to generate the pressure $\tilde{p}_s$. The pressure $\tilde{p}_s$ of the emitted gravity wave at the same time acts on the viscous flow within the lower deck, which is the main source of the radiation. Mathematically, this back-effect on the viscous motion through the pressure gradient is represented by the integral term in the expression for Δ (see (3.35)).

The angle $\phi = \pi/2$ requires some attention. Note that $\phi \to \pi/2$ corresponds to $\xi_0 \gg 1$, for which (Wu & Hogg 2006),

$$\tilde{\mathscr{R}}(\xi_0) \sim -\frac{1}{\xi_0}\left(1 - \xi_0^{-3/2} + O\left(\xi_0^{-3}\right)\right),$$

$$K(\xi + \xi_0, \xi_0) \sim \frac{1}{\xi_0}\left(1 - \xi_0^{-3/2}\mathrm{e}^{-\xi_0^{1/2}\xi} - \xi/\xi_0 + O\left(\xi_0^{-3}\right)\right),$$

for $\xi = O(\xi_0^{-1/2})$. Use of these in (4.16) simplifies it to

$$G_s(\phi; \omega, s) = \tfrac{1}{2}(-\mathrm{i}\omega)^{-5/2} s^{5/2} \mathscr{G}_0 \sin(2\phi), \tag{4.17}$$

where

$$\mathscr{G}_0 = \left\{ \mathrm{i}\omega \widehat{u}'(0)\widehat{F} + (-\mathrm{i}\omega)^{3/2}(-\lambda \widehat{a}\,\widehat{a}_m) + \int_0^\infty \left[\exp(-(-\mathrm{i}\omega)^{1/2} Y) + (-\mathrm{i}\omega)^{1/2} Y\right] H_0(Y)\mathrm{d}Y \right\}, \tag{4.18}$$

with

$$H_0 = \lambda^{-1}\{\mathrm{i}\alpha\lambda(\widehat{u}'\widehat{u}_m - \widehat{u}\,\widehat{u}'_m) + \widehat{u}''[\widehat{u}''_m + \mathrm{i}\alpha\lambda Y \widehat{u}_m + \mathrm{i}\alpha\widehat{p}_m] + \widehat{u}''_m[\widehat{u}'' - \mathrm{i}(\alpha\lambda Y - \omega)\widehat{u} - \mathrm{i}\alpha\widehat{p}]\}.$$

The result (4.17) indicates that the radiated gravity wave tends to zero in the direction $\phi = \pi/2$. It may be worth noting that along this direction, the integral term in Δ is negligible, i.e. the back-effect is insignificant. However, for a general angle ϕ, the back-reaction is a leading-order effect. This is a fundamental difference from the approach based on the extension of acoustic analogy (Stein 1967). The non-physical result that Stein's approach gives has been attributed to the back-action of gravity waves on the source. Evidence of such a feedback effect was also noted in the numerical simulations of gravity waves generated by convectively unstable boundary layers (Clark *et al.* 1986; Hauf & Clark 1989). The present study provides a simple case, for which the back-action has a leading-order effect, and can be elucidated analytically.

4.3. *Numerical result*

To demonstrate the main features of the radiated gravity-wave field, we now present some numerical results for $G_s(\phi; \omega, s)$, performed for topography with a Gaussian shape. Instead of the scaled frequency ω, the familiar non-dimensional frequency, $f = \omega^* \nu / U_\infty^2 \times 10^6$, will be used in the presentation, where ω^* is the dimensional frequency. It may be noted that f is related to ω via

$$f = \omega R^{-3/2} \times 10^6. \tag{4.19}$$

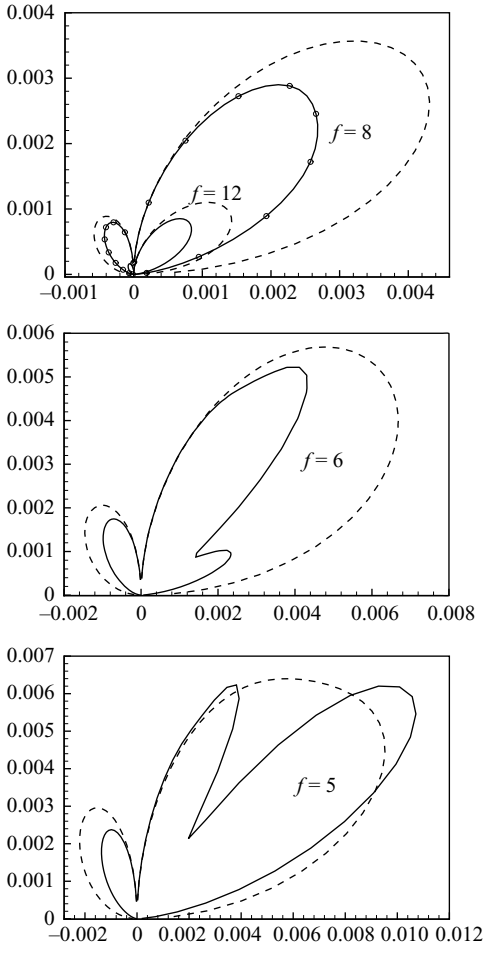

FIGURE 4. The radiated gravity-wave field: $|G_s(\phi, f, s)|$ in polar plots for $f = 12, 8, 6, 5$. The stratification parameter $s = 1$. The dashed lines are plotted according to (4.17).

In all the calculations, we take $d = 4$, $R^2 = 10^7$, and the ω values are chosen to be within the major unstable band of the viscous instability . For convenience, we use the ground shear $\lambda = 0.332$, the value corresponding to the Blasius profile.

The distribution of the radiated gravity wave is shown in figures 4 and 5, where $G_s(\phi; f, s)$ is plotted in polar coordinates for several values of f. Figure 4 is for a case of moderate stratification ($s = 1$), for which the most unstable mode has the frequency $f \approx 8$. The gravity waves appear to be highly directional, consisting of two or three beams, with the main one beamed to the downstream direction. In this moderately stratified case, there is a weak but distinctive beam in the upstream direction. The frequency has an important effect. For relatively high-frequencies, e.g. $f = 8, 12$, there is only one downstream beam. As f is reduced, a new beam starts to emerge in the region close to the x-axis. Finally, the new beam becomes the dominant one. Meanwhile, the overall radiation becomes stronger as f is reduced.

Figure 5 shows the result for $s = 3$. In this case of increased stratification, the upstream beams disappear. For relatively low frequencies (e.g. $f = 6.8$ and 10 (the most unstable mode)), the gravity wave concentrates in one downstream direction.

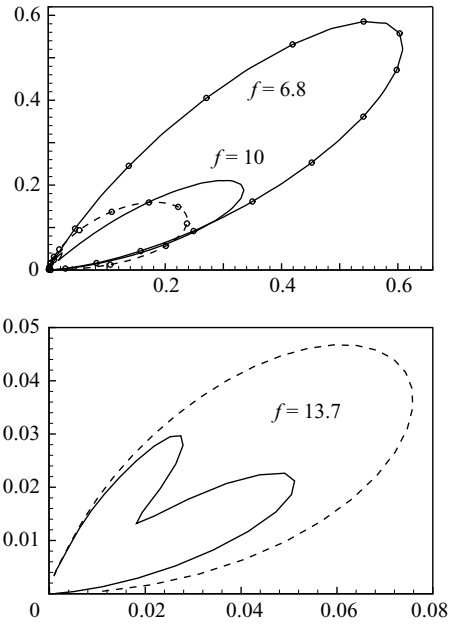

FIGURE 5. The radiated gravity-wave field: $|G_s(\phi; f, s)|$ in polar plots for $f = 6.8, 10, 13.7$. The stratification parameter $s = 3$. The dashed lines are plotted according to (4.17).

However for high frequencies, two beams appear, but the radiated gravity waves become much weaker.

The contrast between figures 4 and 5 implies that stratification has a strong effect on both the directivity and intensity of the radiated gravity waves. As s is increased, the intensity of the gravity wave increases rapidly. Also displayed in figures 4 and 5 are the predictions by (4.17), which is a valid approximation for ϕ close to $\pi/2$. The good agreement in the expected region serves as a useful check of our numerical results.

It should be pointed out that the radiation patterns shown in figures 4 and 5 are, to leading-order, independent of the Reynolds number, provided it is large enough. The Reynolds number only changes the value of f (see (4.19)) at which the pattern is observed. For example, if R is increased by a factor of 100, then the same patterns would appear, but at the frequencies $1/1000$ of those shown in the figures. The Reynolds number chosen ($R = 3.16 \times 10^3$) is several orders of magnitude lower than the values representative of the atmospheric boundary layer, but considerably above the critical Reynolds number for a homogeneous Blasius boundary layer to become unstable. It was chosen in anticipation that a Blasius boundary layer modified by a moderate stratification would be unstable so that controlled experiments, where an instability mode is artificially excited to interact with an isolated roughness, could be performed in the future to validate the theoretical results. Such an experiment would be possible in laboratory facilities such as those described by Ohya & Uchida (2003).

5. Reduced nonlinear system in the high-frequency limit

In the nonlinear case with $h = O(1)$, it is convenient to perform the Prandtl transformation

$$\tilde{Y} = Y - hF, \quad \tilde{U}(X, \tilde{Y}) = U(X, Y), \quad \tilde{V}(X, \tilde{Y}) = V(X, Y) - UhF'(X).$$

Since the boundary-layer equations remain invariant under this transformation, $(\tilde{U}, \tilde{V})$ satisfy (2.6). The boundary and matching conditions are changed to

$$\tilde{U} = \tilde{V} = 0 \quad \text{at} \quad \tilde{Y} = 0; \quad \tilde{U} \to \lambda(\tilde{Y} + A(X,T) + hF(X)) \quad \text{as} \quad \tilde{Y} \to \infty. \tag{5.1}$$

We consider the situation where the oncoming gravity waves are of relatively high frequency, i.e. $\partial/\partial T \sim \Omega \gg O(1)$ (but are still sufficiently slowly varying, i.e. $\Omega \ll O(R^{-1/4})$, to remain quasi-steady in the upper deck). To maintain the balance between the local and convective accelerations, we assume that $\partial/\partial X \sim \Omega^{1/2}$, that is, both the gravity waves and topography vary over a short scale. As in § 5 of Part 1, the flow can be described by the variables

$$\bar{T} = \Omega T, \quad \bar{X} = \Omega^{1/2} X. \tag{5.2}$$

In order to retain the effects of both stratification and topography, the parameters s and h are rescaled as

$$s = \Omega^{1/2}\bar{s}, \quad h = \Omega^{1/2},$$

with $\bar{s} = O(1)$. The lower deck now splits to an inviscid buffer layer and a viscous sublayer. In the buffer layer, $\tilde{Y} = O(\Omega^{1/2})$ and so we introduce $Z = \Omega^{-1/2}\tilde{Y}$. The solution expands as

$$(\tilde{U}, \tilde{V}, P, A) = (\Omega^{1/2}U^*, \Omega^{3/2}V^*, \Omega P^*, \Omega^{1/2}A^*) + \cdots \tag{5.3}$$

with (U^*, V^*, P^*) satisfying (5.3) in Part 1. Then

$$U^* = \lambda(Z + A^* + F), \quad V^* = -\lambda(A^*_{\bar{X}} + F_{\bar{X}})Z \tag{5.4}$$

is an acceptable solution provided that A^* and P^* satisfy

$$\lambda A^*_{\bar{T}} + \lambda^2(A^* + F)(A^* + F)_{\bar{X}} + \frac{\partial}{\partial \bar{X}} \int_{-\infty}^{\infty} \mathscr{G}(\bar{X};\xi)(A^*_{\xi\xi} + \bar{s}^2 A^*)\,\mathrm{d}\xi = -2P_{\mathscr{I},\bar{X}},$$

which, on eliminating λ from the left-hand side via substitution $A^* = \lambda^{-2}A^\dagger$, $F = \lambda^{-2}F^\dagger$ and $\bar{T} = \lambda T^\dagger$, simplifies to

$$A^\dagger_{T^\dagger} + (A^\dagger + F^\dagger)(A^\dagger + F^\dagger)_{\bar{X}} + \frac{\partial}{\partial \bar{X}} \int_{-\infty}^{\infty} \mathscr{G}(\bar{X};\xi)(A^\dagger_{\xi\xi} + \bar{s}^2 A^\dagger)\,\mathrm{d}\xi = -2\lambda^2 P_{\mathscr{I},\bar{X}}. \tag{5.5}$$

It is informative to decompose $A^\dagger$ as a sum of steady and unsteady parts,

$$A^\dagger = \tilde{A} + (A_s - F^\dagger)$$

where the steady part A_s, corresponding to the topography-generated local mean-flow distortion, satisfies

$$\tfrac{1}{2}A_s^2 + \int_{-\infty}^{\infty} \mathscr{G}(\bar{X};\xi)(A_{s,\xi\xi} + \bar{s}^2 A_s)\,\mathrm{d}\xi = \int_{-\infty}^{\infty} \mathscr{G}(\bar{X};\xi)(F^\dagger_{\xi\xi} + \bar{s}^2 F^\dagger)\,\mathrm{d}\xi.$$

The unsteady motion is then governed by

$$\tilde{A}_{T^\dagger} + \tilde{A}\tilde{A}_{\bar{X}} + (A_s\tilde{A})_{\bar{X}} + \frac{\partial}{\partial \bar{X}} \int_{-\infty}^{\infty} \mathscr{G}(\bar{X};\xi)(\tilde{A}_{\xi\xi} + \bar{s}^2\tilde{A})\,\mathrm{d}\xi = -2\lambda^2 P_{\mathscr{I},\bar{X}}. \tag{5.6}$$

In the absence of topography ($F = A_s = 0$), this is a forced extended BDO equation, with incoming gravity waves appearing as a natural physical source. When topography is present, the equation has an additional term $(A_s\tilde{A})_{\bar{X}}$ so that the coefficients now depend on $\bar{X}$. Obviously topography acts as a scatter. Equation (5.6) provides a relatively simple framework to study *nonlinear response* of the boundary layer to

gravity waves, with or without topography. Gravity waves propagate at a common speed c, if their streamwise and vertical wavenumbers, α and β, obey the relation $\alpha^2 + \beta^2 = s^2/(1-c)$. A wavepacket consisting of these components may provoke within the boundary layer, disturbances which are synchronized in phase and hence may appear like a solitary wave. Equation (5.6) also describes nonlinear scatting of an oncoming instability wave or wavepacket. These topics are worth further study.

6. Summary and concluding remarks

As an integral part of our investigation of instability and waves in a stratified boundary layer, we demonstrated that the viscous instability modes described in Part 1 are intrinsically coupled with internal gravity waves in the presence of a localized topography. The two-way coupling involves two fundamental physics processes, receptivity and radiation. On the one hand, gravity waves originating from a distant source can interact with the topography-induced local distortion to excite instability modes. Conversely, boundary-layer instability modes, on approaching a topography, can be scattered into gravity waves. Two further interesting findings were made in the present study: (*a*) gravity waves impinging on the boundary layer almost vertically can be over-reflected; and (*b*) the radiated gravity waves are found to interfere with the source.

Interpreted in the context of the atmospheric boundary layer, the present theoretical results suggest that several specific phenomena could be observed. For instance, when gravity waves in moving air propagate over a hill, spatially growing waves are expected in the downstream region. Such a receptivity process may play a role in triggering intermittency in nocturnal boundary layers. Likewise, when instability waves approach a hill, we may expect to observe considerable gravity waves, possibly in the form of distinct beams, being emitted from the lee side of the hill. Interaction of instability waves with a mountain has been reported by Reinking *et al.* (2003). However, the instability waves were of K-H type, and the attention was on the flow upstream of the mountain. Although gravity-wave generation has been a topic of a great deal of interest, past field investigations have not focused on the specific scenario of radiation due to instability waves interacting with topography as described in the present study. The relevance of receptivity in the atmospheric wave motions does not appear to have been explicitly recognized. Instability itself has often been viewed as triggering the excitation process; the crucial role of scale conversion has not been realized. We hope that the present theoretical work will provide some stimulus and new focus for further field observations.

The coupling with freely propagating gravity waves facilitates long-range effects: a distant event may trigger a major local flow activity and *vice versa*. Such a two-way coupling implies that there is an active exchange of momentum and energy between the regions inside and outside the atmospheric boundary layer. This may have important implications for parameterizing the boundary-layer effect on the general circulation of the atmosphere. Although in the present study, the coupling with internal gravity waves via topography is demonstrated for the viscous instability modes, the scenario and physical concepts are believed to be general. Inviscid instability modes of K-H type are likely to be coupled with gravity waves as well via topography. Such receptivity and radiation problems concerning K-H instability waves require further investigations.

The authors would like to thank the referees for numerous helpful suggestions and for pointing out some key references. Most importantly, their careful scrutiny has helped the authors correct a significant error in the original manuscript.

This research was supported by the Natural Science Foundation of China (grant NSFC/10428206).

REFERENCES

Abramowitz, M. & Stegun, I. A. 1964 *Handbook of Mathematical Functions*. National Bureau of Standards.

Acheson, D. J. 1976 On over-reflexion. *J. Fluid Mech.* **77**, 433–472.

Booker, J. R. & Bretherton, F. P. 1967 The critical layer for internal gravity waves in a shear layer. *J. Fluid Mech.* **27**, 513–539.

Breeding, R. J. 1971 A nonlinear investigation of critical layers for the internal atmosphere gravity waves. *J. Fluid Mech.* **50**, 545–563.

Chimonas, G. & Grant, J. R. 1984 Shear excitation of gravity waves. Part II: Upscale scattering from Kelvin–Helmoholtz waves. *J. Atmos. Sci.* **41**, 2278–2288.

Clark, T. L., Hauf, T. & Kuettner, J. P. 1986 Convectively forced internal gravity waves: results from two-dimensional numerical experiments. *Q. J. R. Met. Soc.* **112**, 899–925.

Coulter, R. L. & Doran, J. C. 2002 Spatial and temporal occurrence of intermittent turbulence during CASES-99. *Boundary-Layer Met.* **105**, 329–349.

Davis, P. A. & Peltier, W. R. 1979 Some characteristics of the Kelvin–Helmholtz and resonant overreflection modes of shear flow instability and of their interaction through vortex pairing. *J. Atmos. Sci.* **36**, 2394–2412.

Einaudi, F., Bedard, Jr, A. J. & Finnigan, J. J. 1989 A climatology of gravity waves and other coherent disturbances at the Boulder atmospheric observatory during March–April 1984. *J. Atmos. Sci.* **46**, 303–329.

Eltayeb, I. A. & McKenzie, J. F. 1975 Critical-layer behaviour and wave amplification of a gravity wave incident upon a shear layer. *J. Fluid. Mech.* **72**, 661–671.

Fritts, D. C. 1984 Shear excitation of atmospheric gravity wvaes. Part II: Nonlinear radiation from a shear layer. *J. Atmos. Sci.* **41**, 524–537.

Fritts, D. C. 1989 A review of gravity saturation processes, effects, and variability in the middle atmosphere. *Pure. Appl. Geophys.* **130**, 343–371.

Fritts, D. C. & Luo, Z. 1992 Gravity wave excitation by geostrophic adjustment of the jet stream. *J. Atmos. Sci.* **49**, 681–697.

Goldstein, M. E. 1985 Scattering of acoustic waves into Tollmien–Schlichting waves by small streamwise variations in surface geometry. *J. Fluid Mech.* **154**, 509–529.

Goldstein, M. E. & Hultgren, L. S. 1989 Boundary layer receptivity to long-wave free-stream turbulence. *Annu. Rev. Fluid Mech.* **21**, 138.

Gossard, E. E. & Hooke, W. H. 1975 *Waves in the Atmosphere*. Elsevier.

Grimshaw, R. H. J. 1981 Resonant over-reflection of internal gravity waves from a thin shear layer. *J. Fluid Mech.* **109**, 349–365.

Hauf, T. & Clark, T. L. 1989 Three-dimensional numerical experiments on convectively forced internal gravity waves. *Q. J. R. Met. Soc.* **115**, 309–333.

Jones, W. L. 1968 Reflexion and stability of waves in stably stratified fluids with shear flow: a numerical study. *J. Fluid Mech.* **34**, 609–624.

Lalas, D. P. & Einaudi, F. 1976 On the characteristics of gravity waves generated by atmospheric shear layer. *J. Atmos. Sci.* **33**, 1248–1259.

Lighthill, M. J. 1952 On sound generated aerodynamically. *Proc. R. Soc. Lond.* A **211**, 564–587.

Lindzen, R. S. 1981 Turbulence and stress owing to gravity wave and tidal breakdown. *J. Geophys. Res.* **86**, 9707–9714.

Lindzen, R. S. & Barker, J. W. 1985 Instability and wave over-reflection in stably stratified shear flow. *J. Fluid Mech.* **151**, 189–217.

Lott, F., Kelder, H. & Teitelbaum, H. 1992 A transition from Kelvin–Helmholtz instabilities to propagating instabilities. *Phys. Fluids* A **4**(9), 1990–1997.

McIntyre, M. E. & Weissman, M. A. 1978 On radiating instabilities and resonant overreflection. *J. Atmos. Sci.* **35**, 1190–1196.

Mastrantonio, G., Einaudi, F., Fua, D. & Lalas, D. P. 1976 Generation of gravity waves by jet streams in the atmosphere. *J. Atmos. Sci.* **33**, 1730–1738.

Nakmura, R. & Mahrt, L. 2005 A study of intermittent turbulence with CASES-99 tower measurements. *Boundary-Layer Met.* **114**, 367–387.

Ohya, Y. & Uchida, T. 2003 Turbulence structure of stable boundary layers with a linear temperature profile. *Boundary-Layer Met.* **108**, 19–38.

Reinking, R. F., Frisch, A. S., Orr, B. W., Korn, D. L., Bissonnette, L. R. & Roy, G. 2003 Remote sensing observation of effects of moutain blocking on travelling gravity-shear waves and associated clouds. *Boundary-Layer Met.* **109**, 255–284.

Ruban, A. I. 1984 On the generation of Tollmien–Schlichting waves by sound. *Fluid Dyn.* **19**, 709–716.

Scinocca, J. F. & Ford, R. 2000 The nonlinear forcing of large-scale internal gravity waves by stratified shear instability. *J. Atmos. Sci.* **57**, 653–672.

Smith, R. B. 1979 The influence of mountains on the atmosphere. *Adv. Geophys.* **21**, 87–230.

Stein, R. F. 1967 Generation of acoustic and gravity waves by turbulence in an isothermal stratified atmosphere. *Solar Phys.* **2**, 385–432.

Stewartson, K. 1974 Multistructured boundary layers on flat plates and related bodies. *Adv. Appl. Mech.* **14**, 145–239.

Sun, J., Burns, S. P., Lenschow, D. H., Banta, R., Newsom, R., Coulter, R., Frasier, S., Ince, T., Nappo, C., Cuxart, J., Blumen, W., Lee, X. & Hu, X. 2002 Intermittent turbulence associated with a density current passage in the stable boundary layer. *Boundary-Layer Met.* **105**, 199–219.

Sun, J., Lenschow, D. H., Burns, S. P., Newsom, R., Coulter, R., Frasier, S., Ince, T., Nappo, C., Balsley, R. B., Jensen, M., Mahrt, L., Miller, D. & Skelly, B. 2004 Atmospheric disturbances that generate intermittent turbulence in nocturnal boundary layers. *Boundary-Layer Met.* **110**, 255–279.

Sykes, R. I. 1978 Stratified effects in boundary layer flow over hills. *Proc. R. Soc. Lond.* A. **361**, 225–243.

Sykes, R. I. 1980 On three-dimensional boundary layer flow over surface irregularities. *Proc. R. Soc. Lond.* A **373**, 311–329.

Wu, X. 2001 On local boundary-layer receptivity to vortical disturbances in the free stream. *J. Fluid Mech.* **449**, 373–393.

Wu, X. & Hogg, L. 2006 Acoustic radiation of Tollmien–Schlichting waves as they undergo rapid distortion. *J. Fluid Mech.* **550**, 303–347.

Wu, X. & Zhang, J. 2008 Instability of a stratified boundary layer and its coupling with internal gravity waves. Part 1. Linear and nonlinear instabilities. *J. Fluid Mech.* **595**, 379–408.